Inorganic Chemistry

pubs.acs.org/IC Article

Linkage Isomers of 4-Methylimidazolate Mn(II) Porphyrinates: Hindered or Unhindered?

Jianping Zhao, Fei Qian, Wenping Guo, Jianfeng Li,* and Zeyuan Lin

Cite This: *Inorg. Chem.* 2021, 60, 7465−7474 Read Online

ACCESS | Metrics & More | Article Recommendations | Supporting Information

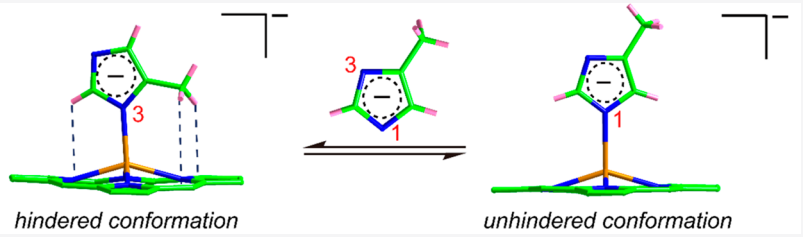

ABSTRACT: Three different manganese(II) porphyrins have been exploited to react with 4-methylimidazolate (4-MeIm$^-$), and the five-coordinate products are characterized by ultraviolet−visible, single-crystal X-ray, and electronic paramagnetic resonance spectroscopies. Interestingly, 4-MeIm$^-$ is found to bond to the metal center through either of the two N atoms (N1 or N3), which yielded two linkage isomers with either an unhindered or a hindered ligand conformation, respectively. Investigations revealed it is the large metal out-of-plane displacements (Δ_{24} and $\Delta_4 \geq 0.59$ Å) that have rendered the equivalence of two isomers with a small energy difference (5.2−8.3 kJ/mol). The nonbonded intra- and intermolecular interactions thus become crucial factors in the balance of linkage isomerization. All of the products in both solution and solid states show the same characteristic resonances of high-spin Mn(II) ($S = {}^5/_2$) with $g_\perp \approx 5.9$ and $g_\parallel \approx 2.0$ at 4 K, consistent with the weak effects of the axial ligand on core conformation and metal electronic configurations. Zero-field splitting parameters obtained through simulations are also reported.

INTRODUCTION

Model compound studies of heme iron are useful for understanding the properties of hemoproteins.[1] Five-coordinate heme iron is involved in a large variety of biological processes, such as catalytic (e.g., cytochrome P450),[2] gas transport (e.g., globins),[3] or signal function (e.g., heme-dependent sensory kinases),[4] allowing interaction of heme with a substrate molecule.[5] The functions of these complexes are modulated by many factors that include the nature and geometry of the axial ligands.[6] Histidyl imidazole that widely exists in five-coordinate heme complexes has been recognized as having a more negative charge than a truly neutral imidazole because of the hydrogen bonding under protein environments.[7] Imidazolate, which is produced by removing the hydrogen of imidazole to give stronger σ and π donation, is the extreme case of strong hydrogen bonding. Thus, imidazolate can be expected to be a stronger field ligand than neutral or H-bonded imidazole. By using 2-methylimidazolate (2-MeIm$^-$) and its precursor 2-methylimidazole (2-MeHIm), both of which have only one hindered ligand conformation through the N2 atom (Scheme 1), several couples of Fe(II) and Co(II) porphyrin adduct products have been synthesized and isolated, respectively.[8,9] Interestingly, as opposed to the case of iron(II) analogues,[8] a complete spin state transition of high-spin ($S = {}^3/_2$) [Co(Porph)(2-MeIm$^-$)]$^-$ and low-spin ($S = {}^1/_2$) [Co(Porph)(2-MeHIm)] was found for Co(II) species that

Scheme 1. Comparison of 2-MeIm$^-$ and 4-MeIm$^-$ (or 5-MeIm$^-$)

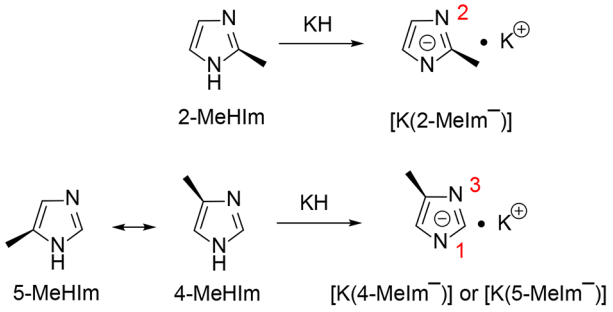

is attributed to the $e_g(d_\pi) \rightarrow b_{1g}(d_{x^2-y^2})$ promotion for the stronger bonding and hindrance of 2-MeIm$^-$.[9,10]

Manganese(II) (d^5) is isoelectronic with iron(III) and, thus, can be employed as a substitute for iron in studying iron-

Received: March 11, 2021
Published: May 5, 2021

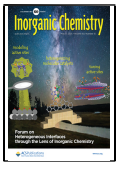

https://doi.org/10.1021/acs.inorgchem.1c00755
Inorg. Chem. 2021, 60, 7465−7474

Table 1. Complete Crystallographic Details for [K(222)][Mn(TPP)(4-MeIm$^-$)]·PhCl, 2{[K(222)][Mn(TTP)(4-MeIm$^-$)]}·3PhCl, [K(222)][Mn(TTP)(4-MeIm$^-$)]·PhCl·H_2O, and [K(222)][Mn(TMP)(4-MeIm$^-$)]·PhCl

	[K(222)][Mn(TPP)(4-MeIm$^-$)]·PhCl	2{[K(222)][Mn(TTP)(4-MeIm$^-$)]}·3PhCl	[K(222)][Mn(TTP)(4-MeIm$^-$)]·PhCl·H_2O	[K(222)][Mn(TMP)(4-MeIm$^-$)]·PhCl
chemical formula	$C_{69}H_{71.5}Cl_{0.5}KMnN_8O_6$	$C_{158}H_{169}Cl_3K_2Mn_2N_{16}O_{12}$	$C_{76}H_{83}ClKMnN_8O_7$	$C_{162.67}H_{191.82}ClK_2Mn_2N_{16}O_{12}$
FW	1220.60	2778.51	1349.99	2786.70
a (Å)	12.3193(8)	28.831(11)	12.9163(5)	12.7623(5)
b (Å)	21.6450(12)	16.886(7)	21.9010(8)	24.3339(11)
c (Å)	23.4929(15)	32.208(12)	24.8329(9)	24.9279(11)
α (deg)	90	90	90	90
β (deg)	96.599(2)	96.410(14)	100.749(2)	90
γ (deg)	90	90	90	90
V (Å^3)	6222.9(7)	15583(11)	6901.5(4)	7741.5(6)
space group	$P21/n$	$C1c1$	$P21/c$	$P212121$
Z	2	4	4	2
crystal color	dark green	dark green	dark green	dark green
crystal dimensions (mm)	0.97 × 0.21 × 0.16	0.59 × 0.26 × 0.12	0.49 × 0.16 × 0.07	0.74 × 0.70 × 0.45
temp (K)	100(2)	100(2)	100(2)	100(2)
total no. of data collected	120489	96267	67069	168308
no. unique data	13253 (R_{int} = 0.1056)	31066 (R_{int} = 0.0736)	14127 (R_{int} = 0.0853)	16494 (R_{int} = 0.0482)
no. of unique observed data [$I > 2\sigma(I)$]	11130	27309	8878	14562
goodness of fit (based on F^2)	1.069	1.028	0.995	1.599
D_{calcd} (g cm^{-3})	1.303	1.184	1.300	1.195
μ (mm^{-1})	0.360	0.329	0.351	0.297
final R indices [$I > 2\sigma(I)$]	R_1 = 0.0627, wR_2 = 0.1593	R_1 = 0.0709, wR_2 = 0.1844	R_1 = 0.0812, wR_2 = 0.2015	R_1 = 0.0637, wR_2 = 0.1870
final R indices (all data)	R_1 = 0.0757, wR_2 = 0.1708	R_1 = 0.0802, wR_2 = 0.1904	R_1 = 0.1381, wR_2 = 0.2421	R_1 = 0.0767, wR_2 = 0.1998

containing heme proteins.[11] Scheidt and co-workers reported the first Mn(II) porphyrin structure in 1977.[12] The high-spin ($S = {}^5/_2$) [Mn(TPP)(1-MeIm)] has a large metal out-of-plane distance (Δ_{24} and $\Delta_4 \geq 0.51$), and the authors suggested that when the $d_{x^2-y^2}$ orbital is populated, the metal atom is too far out of the porphyrin plane to permit effective interaction with a sixth ligand.[12] Thus, Mn(II) porphyrins have a distinct preference to form five-coordinate but not six-coordinate complexes, in contrast to its near neighbors Fe(II) and Fe(III) where a sterically hindered ligand, e.g., 2-methylimidazole, has to be used to prevent the strong tendency to form six-coordinate products.[8,13] In this paper, we report the isolation and characterization of the first examples of imidazolate-ligated Mn(II) porphyrinates [K(222)][Mn(Porph)(4-MeIm$^-$)] (Porph = TPP, TTP, or TMP). Interestingly, linkage isomers with either hindered or unhindered ligand conformations are found for the same porphyrin complex. All of the products are determined to be in the high-spin state, which is consistent with cyanide[14]- and imidazole[15]-ligated Mn(II) analogues.

EXPERIMENTAL SECTION

General Information. All experimental operations with Mn(II) complexes, including the reduction of Mn(III) complexes, were carried out using standard Schlenk ware and cannula techniques under an atmosphere of argon unless otherwise noted. Benzene and tetrahydrofuran (Sinopharm Chemical Reagent) were distilled over sodium/benzophenone. Chlorobenzene (Sinopharm Chemical Reagent) was distilled over P_2O_5 under nitrogen. Hexanes (Beijing Chemical Works) were distilled over a potassium−sodium alloy. 2,6-Dimethylpyridine was purified by being distilled before use. $MnCl_2$, dichloromethane, hydrochloric acid, DMF, and propionic acid were used as received. KH (Aladdin chemicals) was stored in the drybox and washed with hexanes before use. Kryptofix 222 (ACROS) was purified by vacuum sublimation. Potassium 4-methylimidazolate {[K(4-MeIm$^-$)]} was prepared according to the method of Hu et al.[16] The free base H_2TPP and H_2TTP were prepared according to the method of Adler et al.,[17] and H_2TMP was made with a modified procedure published by Lindsey et al.[18] Ultraviolet−visible (UV−vis) spectra were recorded on a PerkinElmer Lambda 25 UV−vis spectrometer.

Synthesis of [Mn(Porph)Cl]. H_2TPP (2 g, 3.26 mmol), 2,6-lutidine (1 mL), and anhydrous $MnCl_2$ (4.07 g, 32.60 mmol) in THF (200 mL) were heated to reflux under argon. The reaction was completed in 6 h. The mixture was dried on a rotary evaporator and extracted with CH_2Cl_2. The filtrate was treated with a diluted HCl solution and then washed with distilled water three times, dried over anhydrous magnesium sulfate, filtered, and evaporated to dryness. The resulting solid was chromatographed on a column of silica gel (2.5:1 benzene/diethyl ether). The first fraction was collected to give 1.4 g of [Mn(TPP)Cl] (61%). Reaction procedures similar to the synthesis of [Mn(TTP)Cl] and [Mn(TMP)Cl] were performed.

Synthesis of [Mn(Porph)(OH)]. A CH_2Cl_2 (100 mL) solution of [Mn(Porph)Cl] (0.5 g, ∼0.7 mmol) was shaken vigorously with a 4 M KOH solution (200 mL) three times and dried over anhydrous magnesium sulfate. After filtration, the filtrate was dried on a rotary evaporator. The resulting solid was eluted on a column of silica gel with benzene and diethyl ether (2.5:1) and then methanol. The last fraction was collected to give 0.3 g of product (62%).

Synthesis of [K(222)][Mn(Porph)(4-MeIm$^-$)]. [Mn(Porph)(OH)] (10 mg, 0.015 mmol) was dried under vacuum for 30 min and dissolved in 5 mL of benzene. After addition of 1 mL of ethanethiol, the solution was stirred for 2 days and evacuated under vacuum to give a purple powder. The purple solid of [Mn(Porph)] (10 mg, 0.015 mmol) was dried for 30 min, and excess [K(4-MeIm$^-$)] (6 mg, 0.050 mmol) and Kryptofix 222 (17 mg, 0.045 mmol) in PhCl (5 mL) were added by cannula. The mixture was stirred for 1 h and transferred into glass tubes (8 mm × 500 mm) that were layered with hexanes as the nonsolvent. Several weeks later, X-ray quality crystals were collected.

X-ray Structure Determination. The single-crystal experiment was carried out on a BRUKER D8 QUEST system with graphite-monochromated Mo Kα radiation (λ = 0.71073 Å). The crystal samples were placed in inert oil, mounted on a glass fiber attached to a brass mounting pin, and transferred to the cold N_2 gas steam of the diffractometer. Crystal data were collected at 100 K and integrated

https://doi.org/10.1021/acs.inorgchem.1c00755
Inorg. Chem. 2021, 60, 7465−7474

using a Bruker Apex II system. The structure was determined by a direct method (SHELXS-2014) and refined against F^2 using SHELXL-2014.[19] Subsequent difference Fourier syntheses led to the location of all remaining non-hydrogen atoms. All non-hydrogen atoms were refined anisotropically if not remarked upon otherwise below. For the structure refinement, all data were used, including negative intensities. All hydrogen atoms were idealized with the standard SHELX idealization methods useless otherwise noted. SADABS[20] was applied for the absorption correction. Complete crystallographic details, atomic coordinates, anisotropic thermal parameters, and fixed hydrogen atom coordinates are given; a brief summary of crystallographic details is given in Table 1.

[K(222)][Mn(TPP)(4-MeIm$^-$)]·PhCl. A dark green crystal with dimensions of 0.97 mm × 0.21 mm × 0.16 mm was used for structure determination. The asymmetric unit contains one porphyrin complex, one potassium cation coordinated with Kryptofix 222, and one PhCl solvent molecule. The PhCl was found to be disordered over two positions, and the final SOFs was refined to be 0.50 and 0.50. Hydrogen atoms H1, H4A, H4B, and H4C were found in Fourier maps, and all coordinates and isotropic temperature factors were refined. Two outliers were omitted in the last cycles of refinement.

2{[K(222)][Mn(TTP)(4-MeIm$^-$)]}·3PhCl. A dark green crystal with dimensions of 0.59 mm × 0.26 mm × 0.12 mm was used for structure determination. The asymmetric unit contains two porphyrin complexes with 4-methylimidazolate ligands, two potassium cations coordinated with Kryptofix 222, and three PhCl solvent molecules. One Kryptofix 222 molecule and one PhCl molecule are disordered. These disordered molecules are restrained by "DFIX", "RIGU", and "ISOR" commands. One region was removed with the SQUEEZE procedure of PLATON after unsuccessful attempts to model it as plausible solvent molecules.

[K(222)][Mn(TTP)(4-MeIm$^-$)]·PhCl·H_2O. A dark green crystal with dimensions of 0.49 mm × 0.16 mm × 0.07 mm was used for structure determination. The asymmetric unit contains one porphyrin complex, one potassium cation coordinated with Kryptofix 222, one PhCl, and one H_2O molecule. PhCl was restrained by "similar U_{ij}" (SIMU) to constrain the anisotropic displacement parameters (ADPs). The H_2O is fully occupied, and two hydrogen atoms are located from the difference Fourier map.

[K(222)][Mn(TMP)(4-MeIm$^-$)]·PhCl. A dark green crystal with dimensions of 0.74 mm × 0.70 mm × 0.45 mm was used for structure determination. The asymmetric unit contains one porphyrin complex, one potassium cation coordinated with Kryptofix 222, and one PhCl solvent molecule. Four carbon atoms (C3, C4, C1A, and C4A) of 4-methylimidazolate and two carbon atoms (C27 and C27A) of the porphyrin phenyl group exhibited unusual thermal motions and, thus, were restrained by the "ISOR" command. PhCl was restrained by "similar U_{ij}" (SIMU) and "DELU" to constrain the anisotropic displacement parameters (ADPs). The disordered 4-methylimidazolate was constrained by means of the "DFIX" command. Twenty-four outliers were omitted in the last cycles of refinement.

EPR Measurements and Simulations. X-Band continuous wave (cw) EPR measurements were carried out on a Bruker EMXPlus/10–12 EPR spectrometer at a microwave frequency of 9.45 GHz using a liquid helium cooling system. The EPR spectra were measured at 4 K with a modulation amplitude of 0.3 mT, a modulation frequency of 100 kHz, and a microwave power of 10.02 mW. [K(222)][Mn(TPP)(4-MeIm$^-$)], [K(222)][Mn(TTP)(4-MeIm$^-$)], and [K(222)][Mn(TMP)(4-MeIm$^-$)] were recorded on both crystalline and solution states, and the solution samples were prepared by mixing [Mn^{II}(Porph)] with 3 equiv of [K(4-MeIm$^-$)] in chlorobenzene. The EPR spectra were simulated to the experimental data using EasySpin,[21] which is operated in MATLAB.

UV–Vis Titration. UV–vis spectra were recorded in a specially designed combined 1 and 10 mm inert atmosphere cell; 1.0 mg (1.5×10^{-3} mmol) of [Mn^{II}(TPP)] was dissolved in 30 mL of THF. The ligand solution (1.5×10^{-2} M) that was prepared by dissolving an equivalent amount of [K(4-MeIm$^-$)] and 222 in THF was titrated into a [Mn^{II}(TPP)] solution, and the UV–vis spectra were measured. Similar procedures were performed for the titrations of [Mn^{II}(TMP)] with [K(4-MeIm$^-$)]. Association constants (K) were derived by the nonlinear curve fitting based on the equations in the Supporting Information.[22]

RESULTS

UV–vis titrations of the 4-MeIm$^-$ ligand to [Mn^{II}(TPP)] were performed, and the spectra are given in Figure 1. As one can see, gradual addition of imidazolate induced Soret (433 nm) and Q bands (568 and 605 nm) to decrease for four-coordinate species, and new bands increase (410, 452, 584, and 627 nm) for the five-coordinate product. Similar results are observed for the titration of [Mn^{II}(TMP)] (Figure 2), which shows new bands at 410, 454, 588, and 630 nm. On the basis of changes in the spectrum, the K values of [K(222)][Mn(TPP)(4-MeIm$^-$)] and [K(222)][Mn(TMP)(4-MeIm$^-$)] were estimated to be $(1.12 \pm 0.2) \times 10^7$ and (3.76 ± 0.2)

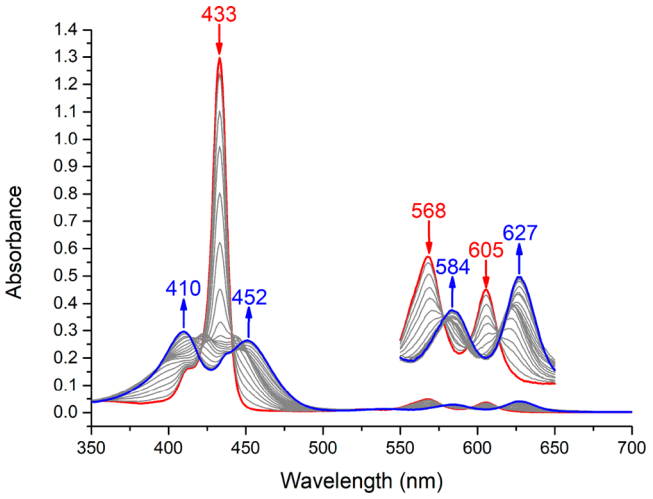

Figure 1. UV–vis spectral change (in THF at 295 K) of a 5×10^{-5} M solution of [Mn^{II}(TPP)] upon gradual addition of [K(4-MeIm$^-$)-(222)]. The enlarged spectra from 550 to 650 nm are measured in the 10 mm UV cell.

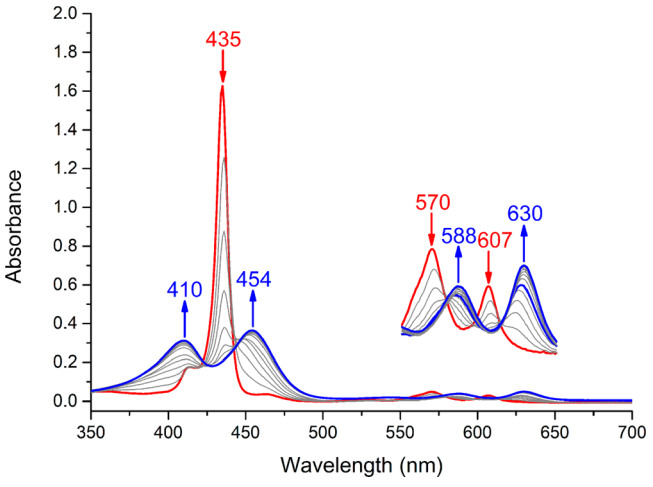

Figure 2. UV–vis spectral change (in THF at 295 K) of a 5×10^{-5} M solution of [Mn^{II}(TMP)] upon gradual addition of [K(4-MeIm$^-$)-(222)]. The enlarged spectra from 550 to 650 nm are measured in the 10 mm UV cell.

https://doi.org/10.1021/acs.inorgchem.1c00755
Inorg. Chem. 2021, 60, 7465–7474

× 10^6 M^{-1}, respectively.[22] It is noteworthy that all of the imidazolate products exhibit two characteristic peaks at ∼410 and 452 nm, in contrast to the imidazole analogues that usually show one Soret band {e.g., 442 nm of [Mn(TpivPP)(2-MeHIm)]}.[15] Because Soret and Q bands are attributed to $a_{1u}(\pi) \rightarrow e_g^*(\pi)$ and $a_{2u}(\pi) \rightarrow e_g^*(\pi)$ transitions, respectively,[23] the distinct spectra suggest different ligand-to-metal and porphyrin-to-metal charge transfer of the two species.[24]

Three different Mn(II) porphyrins (TPP, TTP, and TMP) have been utilized in the reactions with 4-MeIm$^-$, and the products were isolated as single crystals that were determined by 100 K X-ray diffraction. Two crystal forms of TTP derivatives are characterized. In the crystal structure of 2{[K(222)][Mn(TTP)(4-MeIm$^-$)]}·3PhCl, two porphyrin molecules are found in the asymmetric unit and are named [Mn(TTP)(4-MeIm$^-$)]$^-$ (A or B). Thermal ellipsoid plots of these complexes are given in Figure 3. The top-down and edge-on diagrams can be found in Figure S1. Formal diagrams showing the displacements of atoms (in units of 0.01 Å) from the 24-atom mean plane are given in Figure S2. The absolute ligand orientation, given by the dihedral angle between the axial ligand and the closest N_{ax}−M−N_p plane and conventionally denoted by φ, is also shown.

DISCUSSION

Crystal Structures. As one can see in the ORTEP diagrams (Figure 3 and Figure S1), all of the crystal structures are five-coordinate and show apparent metal out-of-plane displacements that indicate the high-spin state of Mn(II). Interestingly, hindered and unhindered linkage isomers are found, which are consistent with the two different bonding sites of 4-MeIm$^-$ (N1 or N3). In crystals of [K(222)][Mn(TPP)(4-MeIm$^-$)]·PhCl and 2{[K(222)][Mn(TTP)(4-MeIm$^-$)]}·3PhCl, 4-MeIm$^-$ bonds to porphyrins in an unexpected hindered conformation with the methyl group directed to the porphyrin planes, similar to a 2-methylimdiaozle(ate) ligand, e.g., [Fe^{II}(TPP)(2-MeHIm)] and [K(222)][Fe^{II}(TPP)(2-MeIm$^-$)].[8] In contrast, crystals of [K(222)][Mn(TMP)(4-MeIm$^-$)]·PhCl and [K(222)][Mn(TTP)(4-MeIm$^-$)]·PhCl·H_2O show the usual unhindered ligand conformation, the same as those of six-coordinate [K(222)][Fe^{III}(TPP)(4-MeIm$^-$)$_2$].[27] The reaction and linkage isomerization are illustrated in Scheme 2.

Table 2 gives key crystal structural parameters of all known imidazole(ate) Mn(II) porphyrinates. Parameters of related Fe(III) analogues are also given for comparisons. The five new structures show consonant structural parameters in narrow ranges, e.g., Δ_{24} and Δ_4 (0.64−0.72 and 0.59−0.64, respectively) and $(Mn-N_p)_{av}$ distances [2.148(15)−2.155(4) Å]. Regardless of the hindered or unhindered conformation, all of the imidazolate Mn(II) derivatives always show larger metal out-of-plane displacements (Δ_{24} and $\Delta_4 \geq 0.59$) and equatorial $(Mn-N_p)_{av}$ distances [≥2.148(15) Å] longer than those of imidazole analogues [Δ_{24} and $\Delta_4 \leq 0.60$; $(Mn-N_p)_{av} \leq$ 2.129(3) Å]. The imidazolate derivatives also show axial Mn−N_{Im} bond distances [≤2.139(5) Å] shorter than those of imidazole analogues [≥2.168(5) Å]. These structural features are quite consistent with the stronger ligand nature of imidazolate than imidazole, which has drawn the metal more out of the porphyrin plane by its stronger bonding.

The steric effect of a hindered axial ligand that would induce larger metal out-of-plane displacements as well as longer (M−$N_p)_{av}$ distances has been widely accepted and, in some cases, applied in the synthesis to obtain five-coordinate high-spin species, e.g., the high-spin iron(II) [Fe(Porph)(2-MeHIm)] complexes.[16] Thus, in Table 2, [Mn(TpivPP)(2-MeHIm)] shows larger Δ_{24} and Δ_4 (0.60 and 0.54, respectively) and longer $(Mn-N_p)_{av}$ distances [2.129(3) Å] than [Mn(TPP)(1-MeIm)], [Mn(TpivPP)(1-MeIm)], and [Mn(TpivPP)(1-EtIm)] that are ligated with unhindered imidazoles. However, this effect is not observed (or tiny, if any) for current imidazolate Mn(II) complexes that already possess large enough metal out-of-plane displacements. [Mn(TMP)(4-MeIm$^-$)]$^-$ with an unhindered ligand, however, shows the largest Δ_4 and $(Mn-N_p)_{av}$ distances, while the expected large parameter values that should have been induced by the hindered 4-MeIm$^-$ of [Mn(TPP)(4-MeIm$^-$)]$^-$ and [Mn-

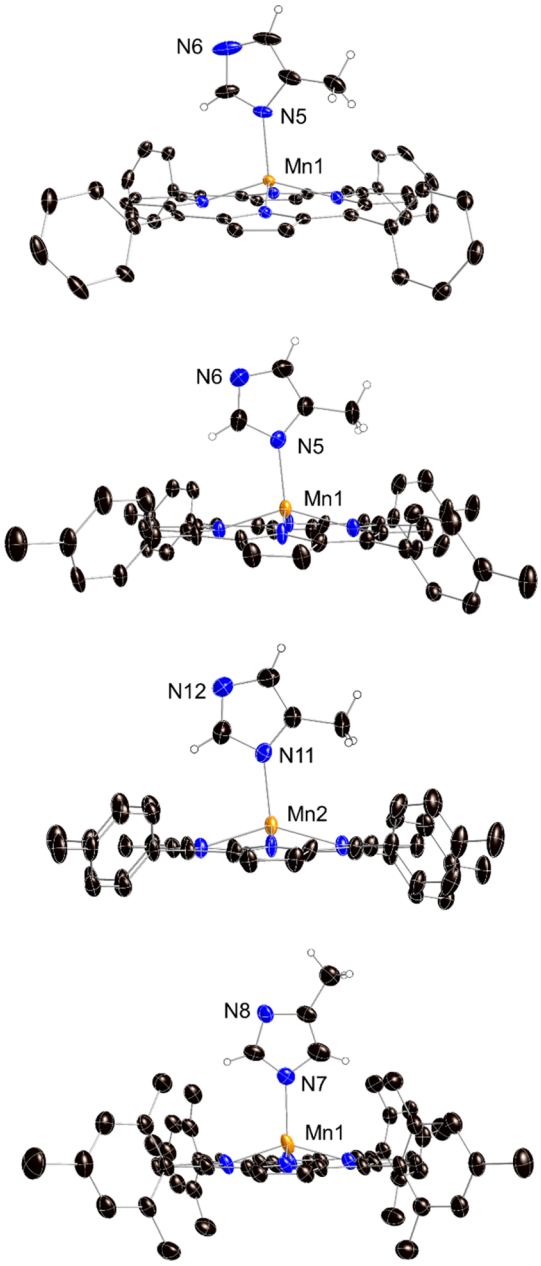

Figure 3. Thermal ellipsoid plots of [Mn(TPP)(4-MeIm$^-$)]$^-$, [Mn(TTP)(4-MeIm$^-$)]$^-$ (A), [Mn(TTP)(4-MeIm$^-$)]$^-$ (B), and [Mn(TMP)(4-MeIm$^-$)]$^-$.

https://doi.org/10.1021/acs.inorgchem.1c00755
Inorg. Chem. 2021, 60, 7465−7474

Scheme 2. Reactions of 4-MeIm$^-$ with Mn(II) Porphyrins

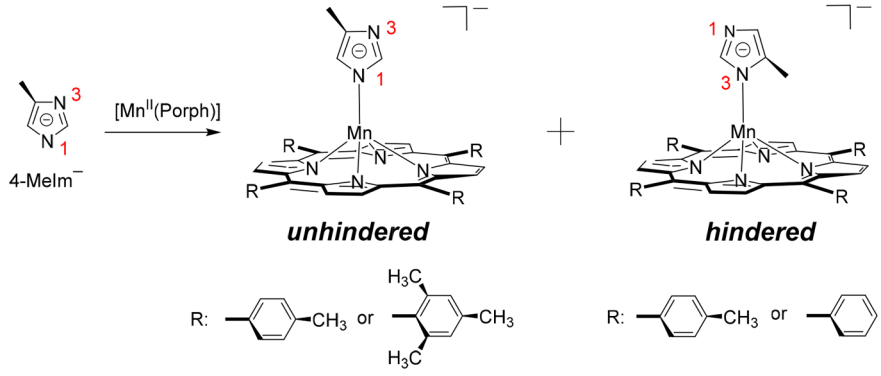

Table 2. Selected Structural Parameters for Manganese(II)/Iron(III) Porphyrin Species

complex	Δ_{24} [a,b]	Δ_4 [a,b]	$(M-N_p)_{av}$ [a,c]	$M-N_{Im}$ [a,d]	$M-N_{Im}-C_{Im}(2)$ [e,f]	$M-N_{Im}-C_{Im}(4)$ [e,g]	φ [e,h]	τ [e,i]	ref
Mn(II) with Hindered Imidazole(ate)									
[Mn(TPP)(4-MeIm$^-$)]$^-$	0.71	0.62	2.153(8)	2.118(2)	133.7(2)	122.44(19)	20.9	4.3	this work
[Mn(TTP)(4-MeIm$^-$)]$^-$ (A)	0.72	0.63	2.152(7)	2.126(6)	132.5(5)	124.6(5)	21.7	6.1	this work
[Mn(TTP)(4-MeIm$^-$)]$^-$ (B)	0.71	0.61	2.148(15)	2.139(5)	134.7(5)	122.0(5)	5.46	6.1	this work
[Mn(TpivPP)(2-MeHIm)]	0.60	0.54	2.129(3)	2.177(9)	126.4(7)	128.1(9)	28.1	9.8	15
Mn(II) with Unhindered Imidazole(ate)									
[Mn(TTP)(4-MeIm$^-$)]$^-$	0.64	0.59	2.150(4)	2.129(4)	125.3(3)	131.5(3)	24.75	12.3	this work
[Mn(TMP)(4-MeIm$^-$)]$^-$ [j]	0.68	0.64	2.155(4)	2.13(21)	122.0(4)	130.0(3)	15.3	3.4	this work
[Mn(TPP)(1-MeIm)]	0.56	0.51	2.128(7)	2.192(2)	130.4(2)	125.2(2)	15.4	10.9	12
[Mn(TpivPP)(1-MeIm)]	0.56	0.50	2.1285(6)	2.168(5)	128.8(9)	125.5(8)	24.0	5.2	15
[Mn(TpivPP)(1-EtIm)] [j]	0.54	0.49	2.122(3)	2.170(7)	130.5(13)	123.0(4)	23.5	5.5	15
Fe(III)									
[Fe(OEP)(2-MeHIm)]ClO$_4$	0.36	0.35	2.038(6)	2.068(4)	131.7(3)	122.1(3)	4.0	5.0	25
[Fe(OEP)(2-MeHIm)]ClO$_4$(A)	0.34	0.34	2.039(28)	2.09	134.6	120.3	7.3	0	25
[Fe(OEP)(2-MeHIm)]ClO$_4$ (B)	0.33	0.31	2.039(28)	2.10	138.2	117.0	3.0	2.5	25
[Fe(oetpp)(2-MeHIm)]ClO$_4$	0.26	0.26	1.966(2)	2.079(2)	132.5(19)	120.5(18)	3.9	2.5	26
[Fe(TPP)(4-MeIm$^-$)$_2$]$^-$	0.00	0.00	1.998(25)	1.928(12)	130.9(11)	127.9(11)	16.7	0	27
				1.958(12)	125.2(11)	129.7(11)	1.4	0	27

[a]Values in angstroms. [b]Displacement of the metal atom from the 24-atom (Δ_{24}) or the four-pyrrole nitrogen atom (Δ_4) mean plane. The positive numbers indicate a displacement toward the axial ligand. [c]Average distance between the metal and porphyrin nitrogen atoms. [d]Distance between the metal and the axial nitrogen atom. [e]Angles in degrees. [f]$M-N_{Im}-C_{Im}$ angle with C2 being the methyl-substituted direction. [g]$M-N_{Im}-C_{Im}$ angle with C4 being the methyl-substituted opposite direction. [h]Dihedral angle between the ligand plane and the plane of the closest N_p-M-N_{Im} angle. [i]Tilt of the $M-N_{Im}$ vector off the normal to the 24-atom mean plane. [j]Average values between two disordered ligand parts.

(TTP)(4-MeIm$^-$)]$^-$ (A and B) are not clear. It is thus deduced that when the metal out-of-plane displacements are large enough (e.g., Δ_{24} and $\Delta_4 \geq 0.59$), the steric effect of hindered 4-MeIm$^-$ is dramatically eliminated, leaving porphyrin cores unaffected. One can also see in Table 2 that the axial distances of picket fence porphyrinates are considerably shorter than those of simple porphyrins [2.168(5)−2.177(9) Å vs 2.192(2) Å]. Similar phenomena have been identified by us for Co(II) and Fe(II) analogues, and we believe it is a specific effect of picket fence porphyrins.[28]

Although both are high-spin states, all of the Mn(II) complexes show metal out-of-plane distances (Δ_{24} and $\Delta_4 \geq 0.49$) that are much larger than those of Fe(III) analogues (0.26−0.36 Å). This is consistent with the ionic radius of Mn(II) being larger than that of Fe(III) (0.66 Å vs 0.49 Å), which does not allow it to fit into the central hole of the porphyrin ring.[29] The smaller metal displacements of iron(III), however, have facilitated tenser axial bonding and presented considerably shorter axial distances [1.928(12)−2.10 Å] compared to those of all of the Mn(II) analogues [2.118(2)−2.192(2) Å].

The tilting of the axial $Mn-N_{Im}$ bond is a partial result of minimizing interactions between imidazole(ate) and the porphyrin plane. Unequal $Mn-N_{Im}-C_{Im}$ angles of imidazole(ate) also serve to minimize the steric interactions. As one can see in Table 2, the hindered Mn(II) complexes have an average value of 131.8° on the methyl side [$M-N_{Im}-C_{Im}(2)$] and 124.3° on the other [$M-N_{Im}-C_{Im}(4)$], and the absolute difference between the two angles ranges from 1.7 to 12.7°, in contrast to the range of 3.0−21.2° for Fe(III) analogues. The much larger angle difference of Fe(III) complexes indicates more steric hindrance that the axial imidazole has suffered, which is thus consistent with its smaller metal displacements as well as tenser and shorter axial distances.

As has been noted, both hindered and unhindered linkage isomers have been isolated from the same reaction of [Mn(TTP)] and 4-MeIm$^-$, the phenomenon of which suggests the two linkage isomers might be very close in energy. Single-point energy calculations on two isomers of each porphyrin were thus conducted, and the results of relative energy at 298.15 K are listed in Table S2. It is seen that although for all three porphyrins, the hindered isomers are predicted to be

https://doi.org/10.1021/acs.inorgchem.1c00755
Inorg. Chem. 2021, 60, 7465−7474

more stable than the unhindered; the energy differences between them are as small as 5.2−8.3 kJ/mol, which speak to a nearly energetic equivalence of linkage isomers. Previously, two crystal forms of ferric bis(imidazole) [Fe(TMP)(5-MeHIm)$_2$]-ClO$_4$ that have different relative ligand orientations (θ) have been isolated and investigated.[30] The *paral*-[Fe(TMP)-(5-MeHIm)$_2$]ClO$_4$ with a θ value of 26° or 30° showed rhombic EPR g tensors (g_1 = 2.69, g_2 = 2.34−2.43, and g_3 = 1.75) and a large quadrupole splitting [ΔE_Q = 2.557(3) mm/s, 120 K], while *perp*-[Fe(TMP)-(5-MeHIm)$_2$]ClO$_4$ with a θ value of 76° showed a single observable g_{max} value (3.43 at 4.2 K) and a small quadrupole splitting [1.78(1) mm/s, 120 K]. Although molecular mechanics calculations indicated nonbonded interactions between the axial ligands and *meso*-mesityl groups destabilize the relative parallel orientation, "the solid-state structure of *paral*-[Fe(TMP)(5-MeHIm)$_2$]ClO$_4$ is observed to be in a hydrogen-bonding network and this feature might be considered responsible for the parallel orientation of the axial ligands".[30] The authors concluded the energy balance between the two isomers is a result of crystal field stabilization effects and steric strain effects, and the two opposing energetic effects are estimated to be both <3.0 kcal/mol (12.55 kJ/mol), which is similar to the range of 5.2−8.3 kJ/mol of current isomers. Therefore, given the same high-spin state (vide infra) and the negatively charged 4-MeIm$^-$ anion ligand that is very likely to interact with its surroundings, various nonbonded forces that play important roles in the balance of linkage isomers are expected for the case presented here.

We first consider the complexes with unusual hindered ligand conformations. Figure 4 illustrates the interactions

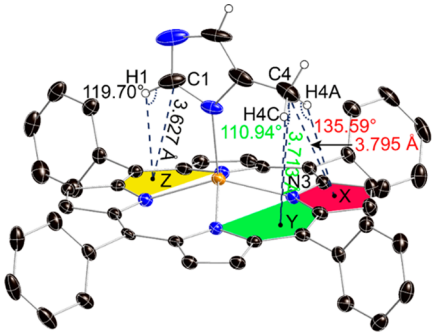

Figure 4. Diagram of [Mn(TPP)(4-MeIm$^-$)]$^-$ showing the geometrical parameters (θ and d) of C−H···π interactions.

between 4-MeIm$^-$ and five-membered atom planes of the porphyrin core of [Mn(TPP)(4-MeIm$^-$)]$^-$. The distances between carbon atoms and the centroid of the close five-membered plane (d) and the C−H···X$_{cent}$ angles (θ) are also given. The corresponding structural parameters of [Mn(TPP)-(4-MeIm$^-$)]$^-$ and [Mn(TTP)(4-MeIm$^-$)]$^-$ (A and B) are summarized in Table S1. As one can see, in a hindered conformation 4-MeIm$^-$ afforded a total of three -CH groups toward the porphyrin core (one from the imidazole hydrogen and two from methyl hydrogens). These -CH groups have d distances (3.625−4.156 Å) of <4.3 Å and θ angles (110.94−140.33°) similar to (or larger than) 120°, in agreement with the existence of nonbonded (C−)H···π interactions.[31]

Similarly, nonbonded interactions are also found for the ligand with the unhindered conformation. In Figure 5, the ORTEP diagram of [K(222)][Mn(TTP)(4-MeIm$^-$)]·PhCl·H$_2$O shows the interactions between 4-MeIm$^-$ and the water

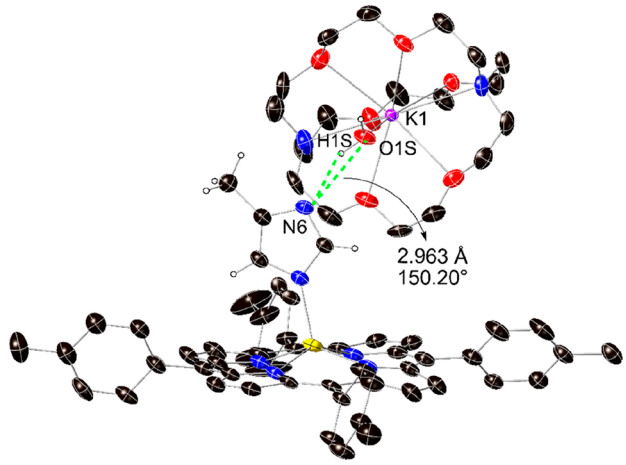

Figure 5. Diagram of [K(222)][Mn(TTP)(4-MeIm$^-$)]·PhCl·H$_2$O showing interactions between 4-MeIm$^-$ and the water molecule bonded to the [K(222)]$^+$ cation.

molecule bonded to the [K(222)]$^+$ cation. As one can see, the [K(222)]$^+$ cation and the [Mn(TTP)(4-MeIm$^-$)]$^-$ anion are quite close to each other, which accounts for the unusually large tilt angle of axial 4-MeIm$^-$ [12.3° (Table 2)] that is induced by the strong steric press of [K(222)]$^+$. The distance between water O1S and N6 of 4-MeIm$^-$ and the corresponding O1S−H1S−N6 angle are 2.963 Å and 150.20°, respectively, in agreement with the (O−)H···N hydrogen bond (e.g., 2.941 Å and 153.0°, respectively).[32] A number of similar intra- and/or intermolecular nonbonded interactions are found for the remaining crystal structures that are illustrated and given in the Supporting Information. As one can see in Figure S5, which illustrates the interactions between the PhCl solvent and 4-MeIm$^-$ ligand of [Mn(TPP)(4-MeIm$^-$)]$^-$, the C2S−N6 distance and C2S−H2S−N6 angle are 3.307 Å and 164.69°, respectively, consistent with a C−H···N interaction.[33] Several C−H···π interactions between PhCl solvents and axial 4-MeIm$^-$ are found for [Mn(TTP)(4-MeIm$^-$)]$^-$ (A and B) and illustrated in Figures S6 and S7.

It is interesting to note the previously reported, six-coordinate bis(4-MeIm$^-$) iron(III) porphyrinate [K(222)]-[Fe^{III}(TPP)(4-MeIm$^-$)$_2$];[27] its synthesis and current Mn(II) products are illustrated in Scheme 3 for comparison. As one can see, 4-MeIm$^-$ could bond to porphyrin metal centers through either N1 or N3, which would yield linkage isomers with an unhindered or a hindered conformation, respectively. In the reaction of Fe(III) species, when 4-MeIm$^-$ bonds through N3, the metal displacements and porphyrin plane deformation required by the steric hindrance of the methyl group make the hindered conformation energetically unfavorable. On the contrary, when 4-MeIm$^-$ bonds through N1, low-spin six-coordinate [K(222)][Fe^{III}(TPP)(4-MeIm$^-$)$_2$] could be formed with unhindered ligands on both porphyrin sides owing to the small ion radius of Fe(III) that allows it to sit inside the porphyrin core. In contrast to Fe(III), Mn(II) with a larger ionic radius always stays outside of the porphyrin core in a high-spin state. As we suggested, the very large metal displacement has dramatically eliminated the steric effect of the methyl group. This feature has allowed 4-MeIm$^-$ to be bonded in either a hindered or an unhindered conformation, resulting in an energetic equivalence of linkage isomers in solution. Under this circumstance, kinds of different intra- and intermolecular nonbonded forces are available to further

https://doi.org/10.1021/acs.inorgchem.1c00755
Inorg. Chem. 2021, 60, 7465−7474

Scheme 3. Reactions of 4-MeIm$^-$ with [Fe^{III}(Porph)]$^+$ and [Mn^{II}(Porph)]

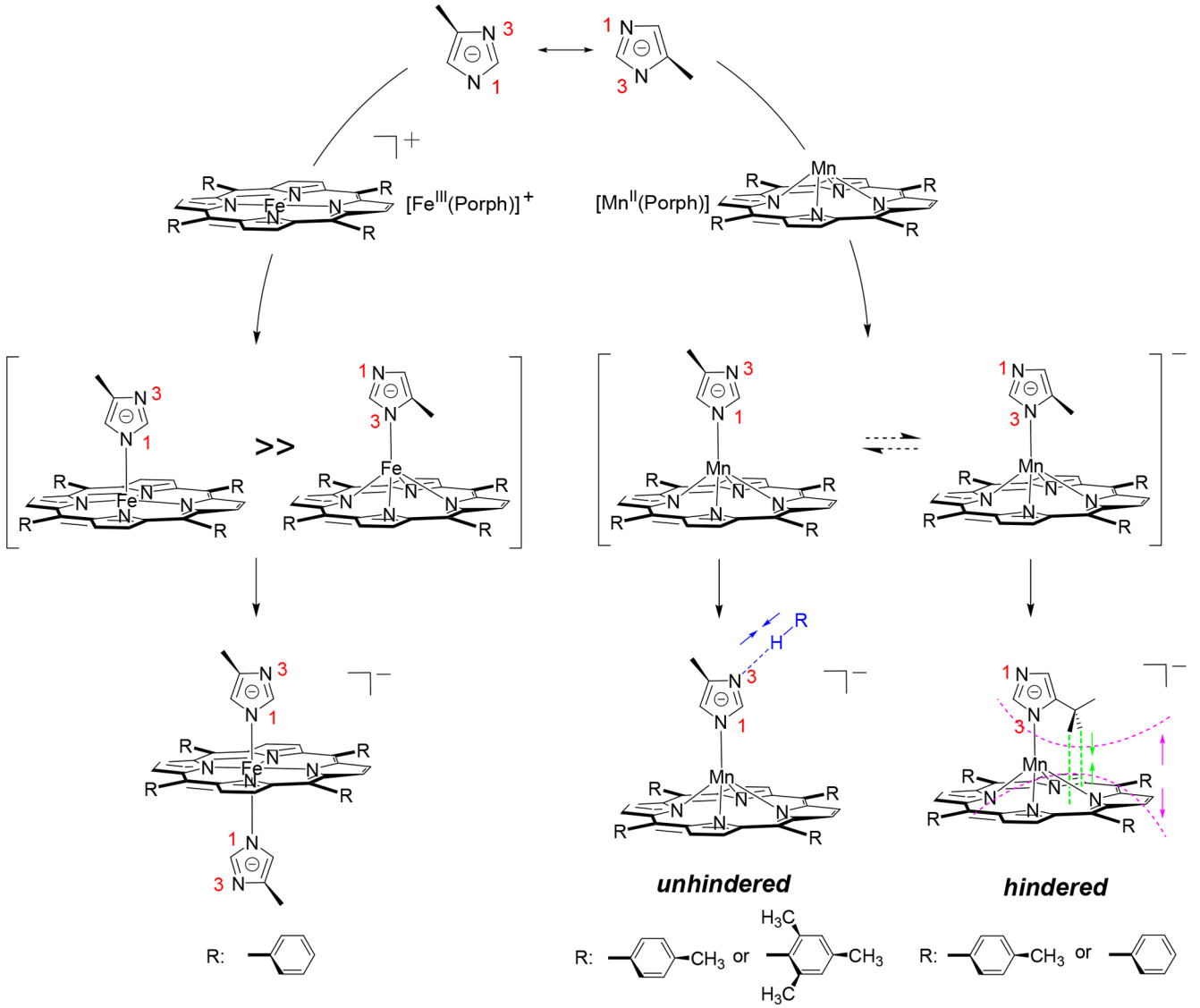

stabilize the products and both isomers can be isolated, e.g., the intermolecular (O−)H···N bond of unhindered [Mn(TTP)(4-MeIm$^-$)]$^-$ (Figure 5). The case of hindered [Mn(TPP)(4-MeIm$^-$)]$^-$ with intramolecular (C−)H···π interactions, however, is very comparable to the known Lennard-Jones potential model of van der Waals interactions, which is a function of the distance between the centers of two atoms (Figure S8).[34] As the separation distance decreases below equilibrium, the potential energy becomes positive, which indicates a repulsive force caused by the overlapping of atomic orbitals. This corresponds to the steric effect of the methyl group in a hindered conformation. However, at long separation distances, the potential energy is negative and approaches zero as the separation distance increases to infinity, which indicates an attractive force. This corresponds to the attractive (C−)H···π interactions of [Mn(TPP)(4-MeIm$^-$)]$^-$ (Figure 4). Finally, as the separation between the two particles reaches a distance where the potential energy reaches a minimum, the pair of particles is most stable and will remain in that orientation until an external force is exerted upon it.[35]

EPR Spectroscopy. X-Band EPR measurements have been performed on all three complexes in both solid and solution states at 4 K, and the spectra are shown in Figure 6. As one can see, all of the spectra show two characteristic signals with $g_\perp \approx 5.9$ and $g_\parallel \approx 2.0$, which are typical of a high-spin ($S = {}^5/_2$) d^5 system [e.g., Fe(III)[36] and Mn(II)[15,37]] and suggest a strong tetragonal field and transitions within the lowest-lying Kramers ($|\pm{}^1/_2\rangle$) doublet.[38] Six lines of hyperfine splittings expected for a Mn(II) nucleus ($I = {}^5/_2$) are seen at $g_\perp \approx 5.9$ for glassy state [Mn(TMP)(4-MeIm$^-$)]$^-$, while it is not well resolved for [Mn(TPP)(4-MeIm$^-$)]$^-$. For all of the solid state samples, hyperfine splittings are not observed. Computer simulations have been performed for [Mn(TMP)(4-MeIm$^-$)]$^-$ to yield spin Hamiltonian parameters. D, E, and the E/D ratio (λ) of related Mn(II) heme complexes are listed in Table 3. As one can see, the D of [Mn(TMP)(4-MeIm$^-$)]$^-$ is slightly smaller than those of the imidazole derivatives (0.67 cm^{-1} vs 0.68 and 0.69 cm^{-1}), and both of them have D values larger than those of the analogues with stronger cyanide and carbene ligands in both solution and solid states.[14,39]

https://doi.org/10.1021/acs.inorgchem.1c00755
Inorg. Chem. 2021, 60, 7465−7474

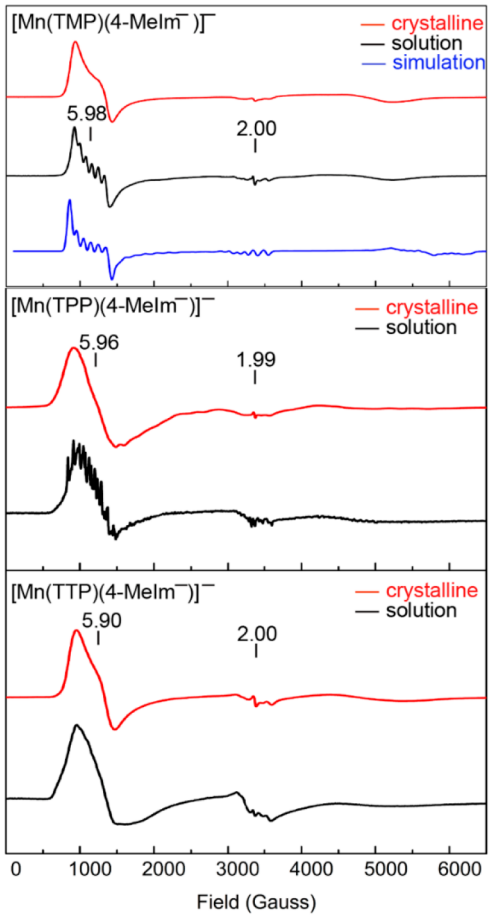

Figure 6. Experimental (red and black lines) and simulated (blue line) X-band EPR spectra of Mn^{II} porphyrinates at 4 K.

CONCLUSIONS

Several single-crystal structures of the first examples of imidazolate-ligated manganese(II) porphyrinates are determined to be five-coordinate and high-spin states. The very large metal out-of-plane displacements of Mn(II) have dramatically eliminated the steric, repulsive interaction between imidazolate and porphyrin cores, which accommodate the hindered or unhindered ligand conformation in the coordination sphere revealing a very unique example of linkage isomerism. The isolation of both crystal forms as well as the consonant high-spin state of all products in both solid and solution states as confirmed by EPR is in agreement with the small energy difference (5.2−8.3 kJ/mol) between the isomers.

ASSOCIATED CONTENT

Supporting Information

The Supporting Information is available free of charge at https://pubs.acs.org/doi/10.1021/acs.inorgchem.1c00755.

Thermal ellipsoid diagrams of [K(222)][Mn(TPP)(4-MeIm⁻)], [K(222)][Mn(TTP)(4-MeIm⁻)] (A), [K(222)][Mn(TTP)(4-MeIm⁻)] (B), [K(222)][Mn(TTP)(4-MeIm⁻)], and [K(222)][Mn(TMP)(4-MeIm⁻)] (Figure S1); formal diagram of the porphyrin core of [K(222)][Mn(TPP)(4-MeIm⁻)], [K(222)][Mn(TTP)(4-MeIm⁻)] (A and B), [K(222)][Mn(TPP)(4-MeIm⁻)], and [K(222)][Mn(TMP)(4-MeIm⁻)] (Figure S2); space filling diagrams (side-on view from the porphyrin plane) of [Mn(TPP)(4-MeIm⁻)]⁻, [Mn(TTP)(4-MeIm⁻)]⁻ (A), and [Mn(TMP)(4-MeIm⁻)]⁻ (Figure S3); X-band EPR spectrum of [K(222)][Mn(TPP)(4-MeIm⁻)] (4 K) (Figure S4); diagrams of [Mn(TPP)(4-MeIm⁻)]⁻ and [Mn(TTP)(4-MeIm⁻)]⁻ (A and B) showing the geometrical parameters (θ and d) of C−H···N or C−H···π interactions (Figures S5−S7); selected structural and C−H···π parameters (Table S1); single-point energy calculations; and a graphical representation of the Lennard-Jones potential (Figure S8) (PDF)

Accession Codes

CCDC 1964144−1964145, 1994678, and 2069670 contain the supplementary crystallographic data for this paper. These data can be obtained free of charge via www.ccdc.cam.ac.uk/data_request/cif, or by emailing data_request@ccdc.cam.ac.uk, or by contacting The Cambridge Crystallographic Data Centre, 12 Union Road, Cambridge CB2 1EZ, UK; fax: +44 1223 336033.

AUTHOR INFORMATION

Corresponding Author

Jianfeng Li − *College of Materials Science and Optoelectronic Technology, CAS Center for Excellence in Topological Quantum Computation, and Center of Materials Science and Optoelectronics Engineering, University of Chinese Academy of Sciences, Beijing 101408, China;* orcid.org/0000-0002-4876-8970; Email: jfli@ucas.ac.cn

Authors

Jianping Zhao − *College of Materials Science and Optoelectronic Technology, CAS Center for Excellence in Topological Quantum Computation, and Center of Materials Science and Optoelectronics Engineering, University of Chinese Academy of Sciences, Beijing 101408, China*

Table 3. EPR Parameters of High-Spin Five-Coordinate Manganese(II) Porphyrin Complexes

complex	g_1	g_2	g_3	g_4	g_5	T^a	phase	$D^{b,c}$	$E^{b,c}$	λ^c	ref
[Mn(TMP)(4-MeIm⁻)]⁻	5.98	2.00				4	solution	0.67	0.00134	0.002	this work
[Mn(TpivPP)(1-MeIm)]	5.94	1.98	1.24	0.78	0.55	90	powder	0.68	0.00338	0.005	15
[Mn(TpivPP)(2-MeHIm)]	5.95	2.0	1.23	0.77	0.54	90	powder	0.69	0.00347	0.005	15
[Mn(TPP)(Py)]	5.96	2.0				77	solution	>0.3		~0.02	37a
Mn-CCP[d]	5.9	2.0	1.21	0.77		77	solution	0.56			37b
[Mn(TPP)(CN)]⁻	5.95	2.00				4	powder	0.53	0.0026	0.005	14
[Mn(TPP)(1,3-Me_2Imd)]	5.95	1.94				90	powder	0.58	0.00696	0.012	39a

[a]Values in kelvin. [b]Values in inverse centimeters. [c]D, E, and λ were estimated from EasySpin simulations. [d]D was estimated from positions of X-band transitions at 77 K; λ was estimated from the number and line shape of hyperfine lines in the X-band transitions at $g_\perp$ = 5.9.

https://doi.org/10.1021/acs.inorgchem.1c00755
Inorg. Chem. 2021, 60, 7465−7474

Fei Qian − *State Key Laboratory of Coal Conversion, Institute of Coal Chemistry, Chinese Academy of Sciences, Taiyuan 030001, China*
Wenping Guo − *National Energy Center for Coal to Liquids, Synfuels China Company, Ltd., Beijing 101400, China*
Zeyuan Lin − *The University of Chinese Academy of Sciences, Beijing 100049, China*

Complete contact information is available at: https://pubs.acs.org/10.1021/acs.inorgchem.1c00755

Notes

The authors declare no competing financial interest.

■ ACKNOWLEDGMENTS

The authors thank the National Natural Science Foundation of China (Grants 21771176 and 21977093 to J.L.). A portion of this work was performed on the Steady High Magnetic Field Facilities, High Magnetic Field Laboratory, CAS. This work is supported in part by the Strategic Priority Research Program of Chinese Academy of Sciences (Grant XDB28000000).

■ REFERENCES

(1) (a) Walker, F. A. Models of the Bis-Histidine-Ligated Electron-Transferring Cytochromes. Comparative Geometric and Electronic Structure of Low-Spin Ferro- and Ferrihemes. *Chem. Rev.* **2004**, *104*, 589−616. (b) Scheidt, W. R.; Reed, C. A. Spin-state/stereochemical relationships in iron porphyrins: implications for the hemoproteins. *Chem. Rev.* **1981**, *81*, 543−555. (c) Adam, S. M.; Wijeratne, G. B.; Rogler, P. J.; Diaz, D. E.; Quist, D. A.; Liu, J. J.; Karlin, K. D. Synthetic Fe/Cu Complexes: Toward Understanding Heme-Copper Oxidase Structure and Function. *Chem. Rev.* **2018**, *118*, 10840−11022.

(2) Cook, D. J.; Finnigan, J. D.; Cook, K.; Black, G. W.; Charnock, S. J. Cytochromes P450: History, Classes, Catalytic Mechanism, and Industrial Application In *Advances in Protein Chemistry and Structural Biology*; Christov, C. Z., Ed.; Elsevier: Amsterdam, 2016; pp 105−126.

(3) Xie, L.-K.; Yang, S.-H. Brain globins in physiology and pathology. *Med. Gas Res.* **2016**, *6*, 154−163.

(4) Ito, Y.; Nakagawa, S.; Komagata, A.; Ikeda-Saito, M.; Shiro, Y.; Nakamura, H. Heme-dependent autophosphorylation of a heme sensor kinase, ChrS, from Corynebacterium diphtheriae reconstituted in proteoliposomes. *FEBS Lett.* **2009**, *583*, 2244−2248.

(5) Baureder, M.; Hederstedt, L. Heme Proteins in Lactic Acid Bacteria. *Adv. Microb. Physiol.* **2013**, *62C*, 1−43.

(6) Zoppellaro, G.; Bren, K. L.; Ensign, A. A.; Harbitz, E.; Kaur, R.; Hersleth, H.-P.; Ryde, U.; Hederstedt, L.; Andersson, K. K. Review: Studies of ferric heme proteins with highly anisotropic/highly axial low spin (S = 1/2) electron paramagnetic resonance signals with bis-Histidine and histidine-methionine axial iron coordination. *Biopolymers* **2009**, *91*, 1064−1082.

(7) (a) Salemme, F. R.; Freer, S. T.; Xuong, N. H.; Alden, R. A.; Kraut, J. The Structure of Oxidized Cytochrome c_2 of Rhodospirillum rubrum. *J. Biol. Chem.* **1973**, *248*, 3910−3921. (b) Landrum, J. T.; Hatano, K.; Scheidt, W. R.; Reed, C. A. Imidazolate complexes of iron and manganese tetraphenylporphyrins. *J. Am. Chem. Soc.* **1980**, *102*, 6729−6735.

(8) Hu, C.; Noll, B. C.; Schulz, C. E.; Scheidt, W. R. Proton-Mediated Electron Configuration Change in High-Spin Iron(II) Porphyrinates. *J. Am. Chem. Soc.* **2005**, *127*, 15018−15019.

(9) Zhao, J.; Peng, Q.; Wang, Z.; Xu, W.; Xiao, H.; Wu, Q.; Sun, H.-L.; Ma, F.; Zhao, J.; Sun, C.-J.; Zhao, J.; Li, J. Proton mediated spin state transition of cobalt heme analogs. *Nat. Commun.* **2019**, *10*, 2303.

(10) Abbreviations: Porph, generalized porphyrin dianion; L, ligand; TPP, meso-tetraphenylporphyrin dianion; TMP, meso-tetramesitylporphyrin dianion; TpivPP, $\alpha,\alpha,\alpha,\alpha$-tetrakis($o$-pivalamidophenyl) porphyrin dianion; OEP, 2,3,7,8,12,13,17,18-octaethylporphyrin dianion; CCP, cytochrome c peroxidase; Hb, hemoglobin; HRP, horseradish peroxidase; Mb, myoglobin; 1-MeIm, 1-methylimidazole; 1-EtIm, 1-ethylimidazole; 2-MeHIm, 2-methylimidazole; 2-MeIm$^-$, 2-methylimidazolate; 4-MeIm$^-$, 4-methylimidazolate; 222 or Krypotofix 222, 4,7,13,16,21,24-hexaoxo-1,10-diazabicyclo[8.8.8]hexacosane; N_p, porphyrin nitrogen; N_{Im}, nitrogen of the imidazole/imidazolate ring; PhCl, chlorobenzene; DMF, *N,N*-dimethylformamide; EPR, electron paramagnetic resonance.

(11) Hoffman, B. M.; Gibson, Q. H.; Bull, C.; Crepeau, R. H.; Edelstein, S. J.; Fisher, R. G.; McDonald, M. J. MANGANESE-SUBSTITUTED HEMOGLOBIN AND MYOGLOBIN*. *Ann. N. Y. Acad. Sci.* **1975**, *244*, 174−186.

(12) Kirner, J. F.; Reed, C. A.; Scheidt, W. R. Stereochemistry of manganese porphyrins. 3. Molecular stereochemistry of $\alpha,\beta,\gamma,\delta$-tetraphenylporphinato(1-methylimidazole)manganese(II). *J. Am. Chem. Soc.* **1977**, *99*, 2557−2563.

(13) Reed, C. A.; Kouba, J. K.; Grimes, C. J.; Cheung, S. K. Manganese(II) and chromium(II) porphyrin complexes: synthesis and characterization. *Inorg. Chem.* **1978**, *17*, 2666−2670.

(14) He, M.; Li, X.; Liu, Y.; Li, J. Axial Mn−C_{CN} Bonds of Cyano Manganese(II) Porphyrin Complexes: Flexible and Weak? *Inorg. Chem.* **2016**, *55*, 5871−5879.

(15) Yu, Q.; Liu, Y.; Liu, D.; Li, J. Geometric and electronic structures of five-coordinate manganese(ii) "picket fence" porphyrin complexes. *Dalton. Trans.* **2015**, *44*, 9382−9390.

(16) Hu, C.; Sulok, C. D.; Paulat, F.; Lehnert, N.; Twigg, A. I.; Hendrich, M. P.; Schulz, C. E.; Scheidt, W. R. Just a Proton: Distinguishing the Two Electronic States of Five-Coordinate High-Spin Iron(II) Porphyrinates with Imidazole/ate Coordination. *J. Am. Chem. Soc.* **2010**, *132*, 3737−3750.

(17) Adler, A. D.; Longo, F. R.; Finarelli, J. D.; Goldmacher, J.; Assour, J.; Korsakoff, L. A simplified synthesis for meso-tetraphenylporphine. *J. Org. Chem.* **1967**, *32*, 476−476.

(18) (a) Wagner, R. W.; Lawrence, D. S.; Lindsey, J. S. An improved synthesis of tetramesitylporphyrin. *Tetrahedron Lett.* **1987**, *28*, 3069−3070. (b) Lindsey, J. S.; Wagner, R. W. Investigation of the synthesis of ortho-substituted tetraphenylporphyrins. *J. Org. Chem.* **1989**, *54*, 828−836.

(19) Sheldrick, G. M. A short history of SHELX. *Acta Crystallogr., Sect. A: Found. Crystallogr.* **2008**, *64*, 112−122.

(20) Krause, L.; Herbst-Irmer, R.; Sheldrick, G. M.; Stalke, D. Comparison of silver and molybdenum microfocus X-ray sources for single-crystal structure determination. *J. Appl. Crystallogr.* **2015**, *48*, 3−10.

(21) Stoll, S.; Schweiger, A. EasySpin, a comprehensive software package for spectral simulation and analysis in EPR. *J. Magn. Reson.* **2006**, *178*, 42−55.

(22) Wu, Z.-Q.; Shao, X.-B.; Li, C.; Hou, J.-L.; Wang, K.; Jiang, X.-K.; Li, Z.-T. Hydrogen-Bonding-Driven Preorganized Zinc Porphyrin Receptors for Efficient Complexation of C60, C70, and C60 Derivatives. *J. Am. Chem. Soc.* **2005**, *127*, 17460−17468.

(23) (a) Gouterman, M. Spectra of porphyrins. *J. Mol. Spectrosc.* **1961**, *6*, 138−163. (b) Wang, D.; Zhang, J.; Shi, T.; Wang, B.; Cao, X.; Li, T. Transition identification of tailed porphyrin-Mn(III) complex in the near-UV and near-IR regions using surface photovoltage spectrum. *J. Photochem. Photobiol., A* **1996**, *93*, 21−25. (c) Zheng, W.; Shan, N.; Yu, L.; Wang, X. UV−visible, fluorescence and EPR properties of porphyrins and metalloporphyrins. *Dyes Pigm.* **2008**, *77*, 153−157.

(24) (a) Boucher, L. J. Manganese porphyrin complexes. *Coord. Chem. Rev.* **1972**, *7*, 289−329. (b) Paulat, F.; Lehnert, N. Detailed Assignment of the Magnetic Circular Dichroism and UV-vis Spectra of Five-Coordinate High-Spin Ferric [Fe(TPP)(Cl)]. *Inorg. Chem.* **2008**, *47*, 4963−4976.

(25) Scheidt, W. R.; Geiger, D. K.; Lee, Y. J.; Reed, C. A.; Lang, G. Characterization of five-coordinate mono(imidazole)(porphinato)-iron(II) complexes. *J. Am. Chem. Soc.* **1985**, *107*, 5693−5699.

(26) Ikezaki, A.; Takahashi, M.; Nakamura, M. Models for Cytochromes c': Observation of an Extremely Labile Spin State in

Monoimidazole Complexes of Saddle-Shaped Iron(III) Porphyrinates. *Angew. Chem., Int. Ed.* **2009**, *48*, 6300−6303.
(27) Quinn, R.; Strouse, C. E.; Valentine, J. S. Crystal structure and properties of a potassium cryptate salt of bis (4-methylimidazolato)-(tetraphenylporphinato) iron (III). *Inorg. Chem.* **1983**, *22*, 3934−3940.
(28) Li, J.; Noll, B. C.; Oliver, A. G.; Ferraudi, G.; Lappin, A. G.; Scheidt, W. R. Oxygenation of Cobalt Porphyrinates: Coordination or Oxidation? *Inorg. Chem.* **2010**, *49*, 2398−2406.
(29) (a) Scheidt, W. R.; Lee, Y. J. Recent advances in the stereochemistry of metallotetrapyrroles. In *Metal Complexes with Tetrapyrrole Ligands*; Buchler, J. W., Ed.; Springer: Berlin, 1987; Vol. *64*, pp 1−70. (b) Shannon, R. Revised effective ionic radii and systematic studies of interatomic distances in halides and chalcogenides. *Acta Crystallogr., Sect. A: Cryst. Phys., Diffr., Theor. Gen. Crystallogr.* **1976**, *32*, 751−767.
(30) Munro, O. Q.; Serth-Guzzo, J. A.; Turowska-Tyrk, I.; Mohanrao, K.; Shokhireva, T. K.; Walker, F. A.; Debrunner, P. G.; Scheidt, W. R. Two Crystalline Forms of Low-Spin [Fe(TMP)(5-MeHIm)$_2$]ClO$_4$. Relative Parallel and Perpendicular Axial Ligand Orientations. *J. Am. Chem. Soc.* **1999**, *121*, 11144−11155.
(31) (a) Brandl, M.; Weiss, M. S.; Jabs, A.; Sühnel, J.; Hilgenfeld, R. C-h···π-interactions in proteins. *J. Mol. Biol.* **2001**, *307*, 357−377. (b) Nishio, M.; Umezawa, Y.; Fantini, J.; Weiss, M. S.; Chakrabarti, P. CH−π hydrogen bonds in biological macromolecules. *Phys. Chem. Chem. Phys.* **2014**, *16*, 12648−12683.
(32) Du, B.; Meyers, E. A.; Shore, S. G. Direct Evidence for O-H···NC Hydrogen Bonding in a Cyanide-Bridged Lanthanide-Transition-Metal Complex $(H_2O)_6(DMF)_6Ho_2[Ni(CN)_4]_3$: An Eight-Coordinated Holmium Center with a Bicapped (Square Face) Trigonal Prismatic Geometry. *Inorg. Chem.* **2000**, *39*, 4639−4645.
(33) (a) Ganesan, S.; Sugumar, P.; Ananthan, S.; Ponnuswamy, M. N. 3,5-Dimethyl-1-{2-[(5-methyl-1,3,4-thiadiazol-2-yl)sulfanyl]-acetyl}-2,6-diphenylpiperidin-4-one. *Acta Crystallogr., Sect. E: Struct. Rep. Online* **2013**, *69*, No. o845. (b) Alshahateet, S. F.; Bishop, R.; Craig, D. C.; Scudder, M. L. Dimeric C−H···N interactions and the crystal engineering of new inclusion host molecules. *CrystEngComm* **2001**, *3*, 225−229.
(34) (a) Jones, J. E.; Chapman, S. On the determination of molecular fields. I. From the variation of the viscosity of a gas with temperature. *Proc. R. Soc. A* **1924**, *106*, 441−462. (b) Jones, J. E.; Chapman, S. On the determination of molecular fields. —II. From the equation of state of a gas. *Proc. R. Soc. A* **1924**, *106*, 463−477. (c) Mueller, J. E.; Fantauzzi, D.; Jacob, T. Multiscale Modeling of Electrochemical Systems. In *Electrocatalysis - Theoretical Foundations and Model Experiments*; Wiley-VCH, 2013; pp 1−74.
(35) Atkins, P.; De Paula, J. Macromolecules and self-assembly. In *Physical Chemistry for the Life Sciences*, 2nd ed.; W. H. Freeman and Co.: New York, 2011; pp 432−436.
(36) (a) Sakai, T.; Ohgo, Y.; Hoshino, A.; Ikeue, T.; Saitoh, T.; Takahashi, M.; Nakamura, M. Electronic Structures of Five-Coordinate Iron(III) Porphyrin Complexes with Highly Ruffled Porphyrin Ring. *Inorg. Chem.* **2004**, *43*, 5034−5043. (b) Matsuo, T.; Dejima, H.; Hirota, S.; Murata, D.; Sato, H.; Ikegami, T.; Hori, H.; Hisaeda, Y.; Hayashi, T. Ligand Binding Properties of Myoglobin Reconstituted with Iron Porphycene: Unusual O_2 Binding Selectivity against CO Binding. *J. Am. Chem. Soc.* **2004**, *126*, 16007−16017. (c) Ikezaki, A.; Nakamura, M. Models for Cytochromes *c*′: Spin States of Mono(imidazole)-Ligated (meso-Tetramesitylporphyrinato)iron-(III) Complexes as Studied by UV-Vis, ^{13}C NMR, ^{1}H NMR, and EPR Spectroscopy. *Inorg. Chem.* **2002**, *41*, 6225−6236. (d) Patra, R.; Bhowmik, S.; Ghosh, S. K.; Rath, S. P. Effects of axial pyridine coordination on a saddle-distorted porphyrin macrocycle: stabilization of hexa-coordinated high-spin Fe(iii) and air-stable low-spin iron(ii) porphyrinates. *Dalton. Trans.* **2010**, *39*, 5795−5806.
(37) (a) Hoffman, B. M.; Weschler, C. J.; Basolo, F. The dioxygen adduct of meso-tetraphenylporphyrinmanganese(II), a synthetic oxygen carrier. *J. Am. Chem. Soc.* **1976**, *98*, 5473−5482. (b) Yonetani, T.; Drott, H. R.; Leigh, J. S.; Reed, G. H.; Waterman, M. R.; Asakura, T. Electromagnetic Properties of Hemoproteins: III. Electron Paramagnetic Resonance Characteristics of Iron (III) and Manganese (II) Protoporphyrins IX and Their Apohemoprotein Complexes in High Spin States. *J. Biol. Chem.* **1970**, *245*, 2998−3003.
(38) Brudvig, G. W. EPR spectroscopy of manganese enzymes. In *Advanced EPR: Applications in Biology and Biochemistry*; Hoff, A. J., Ed.; Elsevier: Amsterdam, 1989; pp 839−863.
(39) (a) Yao, Z.; Li, H.; Liang, X.; Xu, X.; Li, J. The first isolated Manganese(II) porphyrin N-Heterocyclic carbenes: Synthesis and spectroscopic characterizations. *Dyes Pigm.* **2019**, *162*, 75−79. (b) Liu, Y.; Xu, W.; Zhang, J.; Fuller, W.; Schulz, C. E.; Li, J. Electronic Configuration and Ligand Nature of Five-Coordinate Iron Porphyrin Carbene Complexes: An Experimental Study. *J. Am. Chem. Soc.* **2017**, *139*, 5023−5026.

NOTE ADDED AFTER ASAP PUBLICATION

This article posted ASAP on May 5, 2021. Scheme 1 has been updated and the corrected version was reposted on May 17, 2021.

https://doi.org/10.1021/acs.inorgchem.1c00755
Inorg. Chem. 2021, 60, 7465−7474